

THREE-DIMENSIONAL SIMULATIONS OF THE DEFLAGRATION PHASE OF THE GRAVITATIONALLY CONFINED DETONATION MODEL OF TYPE Ia SUPERNOVAE

G. C. JORDAN IV,^{1,2} R. T. FISHER,^{1,2} D. M. TOWNSLEY,^{2,3} A. C. CALDER,^{1,2,4} C. GRAZIANI,^{1,2}
S. ASIDA,⁵ D. Q. LAMB,^{1,2,6} AND J. W. TRURAN^{1,2,6,7}
Received 2007 March 22; accepted 2008 March 11

ABSTRACT

We report the results of a series of three-dimensional (3D) simulations of the deflagration phase of the gravitationally confined detonation mechanism for Type Ia supernovae. In this mechanism, ignition occurs at one or several off-center points, resulting in a burning bubble of hot ash that rises rapidly, breaks through the surface of the star, and collides at a point opposite the breakout on the stellar surface. We find that detonation conditions are robustly reached in our 3D simulations for a range of initial conditions and resolutions. Detonation conditions are achieved as the result of an inwardly directed jet that is produced by the compression of unburnt surface material when the surface flow collides with itself. A high-velocity outwardly directed jet is also produced. The initial conditions explored in this paper lead to conditions at detonation that can be expected to produce large amounts of ⁵⁶Ni and small amounts of intermediate-mass elements. These particular simulations are therefore relevant only to high-luminosity Type Ia supernovae. Recent observations of Type Ia supernovae imply a compositional structure that is qualitatively consistent with that expected from these simulations.

Subject headings: hydrodynamics — nuclear reactions, nucleosynthesis, abundances — supernovae: general — white dwarfs

1. INTRODUCTION

Type Ia supernovae have received increased interest because of their importance as “standard candles” for cosmology. Observations using Type Ia supernovae as standard candles have revealed that the expansion rate of the universe is accelerating and have led to the discovery of “dark energy” (Riess et al. 1998; Perlmutter et al. 1998). But the way in which Type Ia supernovae explode is not completely understood. The current leading paradigms for the explosion mechanism are (1) pure deflagration (Reinecke et al. 2002b; Gamezo et al. 2003; Röpke & Hillebrandt 2005), (2) deflagration-to-detonation transition (DDT; Khokhlov 1991; Gamezo et al. 2004, 2005), (3) pulsational detonation (PD; Khokhlov 1991; Bravo & Garcia-Senz 2006), and (4) gravitationally confined detonation (GCD; Plewa et al. 2004; Livne et al. 2005; Plewa 2007; Townsley et al. 2007). There is increasing evidence that a detonation is needed (Höfllich et al. 2002; Badenes et al. 2006; Wang et al. 2006, 2007; Gerardy et al. 2007), as is posited in the last three models.

A fundamental question has been how the transition to a detonation occurs in a white dwarf (WD) star (see, e.g., Niemeyer 1999). While the DDT, PD, and GCD paradigms incorporate a detonation, all existing DDT simulations invoke the transition to a detonation in an ad hoc fashion, and the PD mechanism re-

mains largely unexplored by detailed simulations. In contrast, extensive two-dimensional (2D) cylindrical simulations have shown that detonation conditions are robustly reached in the GCD model for a variety of initial conditions (Plewa et al. 2004; Plewa 2007; Röpke et al. 2007; Townsley et al. 2007). Thus, to date, the GCD mechanism is the only proposed mechanism for which a detonation has been demonstrated to arise naturally.

However, the achievement of detonation conditions has not been demonstrated in three dimensions (3D; see, e.g., Röpke et al. 2007). This is a concern, since the behavior of turbulence is different in 3D than in 2D, and the cylindrical symmetry of the 2D simulations might enhance the focusing of the surface flow that triggers the detonation in the GCD model. Hence, a major question that we address in this paper is whether it is possible to achieve detonation conditions in a fully 3D simulation of the GCD model. In addition, the large amount of nuclear burning that occurs in the Röpke et al. (2007) simulations appears to play a role in the failure of these simulations to achieve detonation conditions in 3D. In this paper, we report the results of seven 3D simulations of the GCD model for several different sets of initial conditions and two resolutions. We find that the conditions for detonation are robustly achieved for these initial conditions. Thus, the simulations reported in this paper address the first point above and provide a counterexample to the second.

The organization of the paper is as follows. We describe the simulation setup in § 2 and the results of the simulations in § 3. We discuss the properties of Type Ia supernovae expected in the GCD model and compare the results of our simulations with earlier work in § 4. Finally, we state our conclusions in § 5.

2. SIMULATION SETUP

We perform our 3D simulations of the deflagration phase of the GCD model using FLASH 3.0, an adaptive mesh hydrodynamics code (Fryxell et al. 2000; Calder et al. 2002). The general simulation setup is identical to that in the 2D simulations of the

¹ Center for Astrophysical Thermonuclear Flashes, University of Chicago, Chicago, IL 60637.

² Department of Astronomy and Astrophysics, University of Chicago, Chicago, IL 60637.

³ Joint Institute for Nuclear Astrophysics, University of Chicago, Chicago, IL 60637.

⁴ Current address: Department of Physics and Astronomy and New York Center for Computational Science, Stony Brook University, Stony Brook, NY 11794-3800.

⁵ Racah Institute of Physics, Hebrew University, Jerusalem 91904, Israel.

⁶ Enrico Fermi Institute, University of Chicago, Chicago, IL 60637.

⁷ Argonne National Laboratory, Argonne, IL 60439.

GCD model described in Townsley et al. (2007). In particular, the initial model is a $1.365 M_{\odot}$ WD with a uniform composition of equal parts by mass of ^{12}C and ^{16}O . It has a central density of $2.2 \times 10^9 \text{ g cm}^{-3}$, a uniform temperature of $4 \times 10^7 \text{ K}$, and a radius of approximately 2000 km.

The physical thickness of the carbon burning stage of the nuclear flame front in the deflagration phase of Type Ia supernovae is 10^{-4} to 10^3 cm for the densities of interest, and is therefore unresolvable in any whole-star simulation. Consequently, a method must be used to determine the location and speed of the flame front. Two fairly different methods of flame-front tracking have been used in recent studies of WD deflagration. One is the level set technique, in which the location of the flame front is calculated based on the value of a smooth field defined on the grid and propagated with an advection equation acting in addition to the hydrodynamics (Reinecke et al. 1999; Röpke et al. 2003; Röpke & Hillebrandt 2005). This method has been used to study the effect of turbulence on the nuclear burning rate (Schmidt et al. 2006a) and in many simulations of WD deflagration (see, e.g., Reinecke et al. 1999; Röpke & Hillebrandt 2005; Schmidt et al. 2006b). The other method artificially broadens the flame front using a reaction progress variable and propagates it using an advection-diffusion-reaction (ADR) equation (Khokhlov 1995; Vladimirova et al. 2006). This ADR flame model has been used to study the effect of the Rayleigh-Taylor (R-T) instability on a propagating flame front (Khokhlov 1995; Zhang et al. 2007) and in many previous simulations of WD deflagration (Gamezo et al. 2003; Calder et al. 2004; Plewa et al. 2004; Plewa 2007; Townsley et al. 2007).

In this paper, we follow the nuclear flame using a new version (S. Asida et al. 2008, in preparation) of an ADR flame model. The new prescription uses the Kolmogorov-Petrovski-Piskunov (KPP) form of the reaction term in which this term is slightly truncated, as opposed to the top-hat form used previously by ourselves and others (e.g., Khokhlov 1995). This new version is numerically quieter, more stable, and exhibits far smaller curvature effects (S. Asida et al. 2008, in preparation). The thickness of the flame is ≈ 4 grid points; more details and the explicit values of the parameters in the ADR flame model that we use are given in Townsley et al. (2007). We also use a new, acoustically quiet version (Townsley et al. 2007) of the nuclear energy release method described in Calder et al. (2007) that accounts more accurately for the nuclear energy released in the flame and in the evolution of nuclear statistical equilibrium (NSE) as conditions change within the bubble of hot ash.

We do not include nuclear burning outside the flame in the simulations reported in this paper. This approach is the same as that adopted by Röpke et al. (2007). Were we to have included such burning, both the 2D simulations reported in Townsley et al. (2007) and the 3D simulations reported in this paper would detonate at the first instant at which detonation conditions are reached, as we will report in later papers (C. A. Meakin et al. 2008, in preparation; G. C. Jordan et al. 2008, in preparation). Thus, including nuclear burning outside the flame would not have allowed us to demonstrate that the simulations reported in this paper robustly reach conservative conditions for detonation: i.e., that they exceed the temperature and the density needed to detonate for a significant period of time.

We treat the effect of R-T-driven turbulence in the same manner as in Townsley et al. (2007); namely, we impose a minimum flame speed $s_{\min} = \alpha(Agm_f \Delta x)^{1/2}$, where Δx is the grid size of the simulation, $\alpha = 0.5$ is a geometrical factor, and $m_f = 0.06$ is a constant that we have calibrated (Townsley et al. 2007, 2008 [in preparation]). This is a conservative approach that allows the simulation to treat the effects of R-T-driven turbulence on re-

solved scales while ensuring that turbulence on the scale of the (artificially broadened) flame thickness does not disrupt the flame. We disable this prescription in the truncated cone encompassing the region where the surface flow collides with itself to ensure that no unrealistic heating occurs.

If the nuclear burning rate, as well as the overall dynamics of R-T-driven turbulent nuclear burning, are determined by the behavior at large scales, then turbulence at small scales does not increase the burning rate, and the moderate resolution possible in current simulations is adequate. That this may be the case is suggested by the results of Zhang et al. (2007), who find that the time-averaged rate of buoyancy-driven nuclear burning did not vary when the resolution was varied by a factor of 4. Because we rely on the resolution of our simulations to describe turbulent nuclear burning, and therefore the rate of nuclear burning, we have paid close attention to how the rate varies with resolution. We have found no evidence for more than a modest variation of the nuclear burning rate due to unresolved behavior—as we discuss below. However, the appropriate way to treat turbulent nuclear burning is an open question (cf. Reinecke et al. 2002a; Zingale et al. 2005; Schmidt et al. 2006a; Zhang et al. 2007), and further studies are needed in order to definitively answer this question.

The core of the star is thought to be convective and therefore to have velocities on the largest scales of $\sim 100 \text{ km s}^{-1}$ (Woosley et al. 2004; Wunsch & Woosley 2004), which are comparable to the laminar flame speed in this region (Timmes & Woosley 1992). The temperature fluctuations in the convective region may lead to one, to a few, or to many ignition points. The convective motions are likely to distort the ignition region(s), seeding later R-T instability modes. However, the motions are not strong enough to destroy the ignition region(s), once born. In addition, Livne et al. (2005) find that the general outcome of off-center ignitions is not strongly affected by the presence of a convective velocity field. Finally, we would like to understand the behavior of the simpler case of a single, spherical ignition region and zero velocity in the core of the star before considering more complicated cases. For all of these reasons, we adopt a single ignition point at a range of offset distances from the center of the star as the initial conditions in this paper. We will investigate ignition at multiple points and the effects of convective motions in the core of the star in future papers.

We model the ignition region as a spherical bubble of hot ash initially at rest, characterized by an initial radius, r_{bubble} , and an initial distance, r_{offset} , from its center to the center of the star along the z -axis. The edge of the burned region forms a smooth transition from fuel to ash that is ~ 4 zones in width (see Townsley et al. [2007] for more details). The density of the hot ash is chosen to maintain pressure equilibrium with the surrounding material. The surface of the bubble of hot ash corresponds to the $\phi_1 = 0.5$ isosurface, where ϕ_1 is the flame progress variable for $^{12}\text{C} + ^{12}\text{C}$ burning (Townsley et al. 2007). Thus, the radius, r_{bubble} , is approximately the radius of the $\phi_1 = 0.5$ isosurface.

Initially, the spherical bubble of hot ash rises slowly, due to its small size and the small value of the acceleration of gravity g near the center of the star. The growth of the bubble is self-similar—i.e., independent of its initial radius—provided that $r_{\text{bubble}} \lesssim \lambda_c \equiv 6\pi s^2 / Ag$ (Vladimirova 2007; R. Fisher et al. 2008, in preparation). Here r_{bubble} is the initial radius of the bubble, λ_c is the minimum wavelength for the unstable R-T growth of flame surface perturbations, s is the laminar flame speed, $A = (\rho_{\text{fuel}} - \rho_{\text{ash}}) / (\rho_{\text{fuel}} + \rho_{\text{ash}})$ is the Atwood number, and g is the acceleration of gravity at r_{offset} . Otherwise, the initial bubble is immediately unstable to the growth of R-T modes. This is inconsistent with the

TABLE 1
PROPERTIES OF 3D GCD SIMULATIONS

Label	r_{bubble} (km)	r_{offset} (km)	Resolution (km)	$E_{\text{nuc, def}}$ (10^{49} ergs)	M_{heavy} (M_{\odot})	M_{inter} (M_{\odot})	E_{total} (10^{51} ergs)	t_{det} (s)
16b20o8r.....	16	20	8	10.5	1.00	0.36	1.50	2.89
18b42o6r.....	18	42	6	6.7	1.18	0.19	1.57	2.30
16b40o8r.....	16	40	8	6.1	1.20	0.16	1.58	2.38
16b100o8r.....	16	100	8	3.2	1.26	0.10	1.60	2.02
25b100o6r.....	25	100	6	3.0	1.27	0.17	1.60	1.84
25b100o8r.....	25	100	8	3.1	1.26	0.11	1.60	2.01
50b100o8r.....	50	100	8	6.5	1.11	0.25	1.55	2.45

NOTE.—This table gives the properties of the seven 3D simulations of GCD models reported in this paper.

assumption of a small, spherical ignition region. Thus, $r_{\text{bubble}} \lesssim \lambda_c$ for all of the simulations reported in this paper, except for two we conducted to compare with those of Röpke et al. (2007).

The adaptive mesh refinement criteria we use are chosen to capture the relevant physical features of the burning and the flow at reasonable computation expense. The criteria for refinement are the same as those described in Townsley et al. (2007), except that we maximally refine a sphere of radius $r_{\text{refine}} = 1000$ km at the center of the star and a truncated cone encompassing the region where the flow of hot bubble material over the surface of the star collides with itself. The truncated cone has an opening half-angle $\theta_{\text{cone}} = 30^\circ$, and extends from a radius $r_{\text{cone, min}} = 1500$ km to a radius $r_{\text{cone, max}} = 3000$ km.

3. RESULTS

We performed a suite of seven 3D simulations of the deflagration phase of the GCD model for initially stationary, spherical flame bubbles, varying the initial bubble radius r_{bubble} , the initial bubble offset r_{offset} , and the finest resolution. Table 1 lists the initial conditions and several properties of these simulations. The simulations are denoted by initial bubble radius, offset distance, and finest resolution. Thus, 18b42o6r denotes a 3D simulation in which the initial bubble radius $r_{\text{bubble}} = 18$ km, the offset distance $r_{\text{offset}} = 42$ km, and the finest resolution is 6 km.

Our 3D simulations of the GCD model progress similarly to previous 2D GCD simulations (Plewa et al. 2004; Plewa 2007; Townsley et al. 2007), passing through several distinct stages. Initially, the spherical bubble of hot ash that we adopt as our model of the ignition region grows at a rate dictated by the laminar flame speed. At ~ 0.2 – 0.3 s of simulation time, the radius r_{bubble} of the bubble exceeds λ_c , the minimum wavelength for the unstable R-T growth of flame surface perturbations (Khokhlov 1995; Zhang et al. 2007). When this happens, the top surface of the bubble develops a bulge, and the bubble quickly evolves into a mushroom-like shape (Calder et al. 2004; Plewa et al. 2004; Vladimirova 2007; Plewa 2007; Townsley et al. 2007). Subsequently, the shape of the bubble becomes ever more complex as the critical wavelength λ_c becomes smaller (as the bubble rises and g at the position of the bubble increases), and additional generations of smaller features appear as a result of the R-T instability. During this time, the rate at which the bubble rises increases, and the bubble breaks through the stellar surface at ~ 0.8 – 1.2 s. The hot ash in the bubble (which was produced at a range of densities and so consists of both iron peak and intermediate-mass elements) then spreads rapidly over the surface of the star, pushing unburnt material in the outermost layer of the star ahead of it.

The mass of the hot ash from the bubble that sweeps over the surface of the star ranges from 0.038 to 0.010 M_{\odot} for offset distances of the initial bubble ranging from 20 to 100 km. Its com-

position ranges from roughly 0.009 to 0.002 M_{\odot} of intermediate-mass elements and roughly 0.007–0.03 M_{\odot} of Fe peak elements for these offset distances. However, we caution that the present simulations do not seek to accurately treat mixing between the ash flow across the surface of the star and the underlying outermost layers of the WD, which will significantly affect the final composition of these layers.

At ~ 1.8 – 2.2 s, the flow of hot ash collides with itself at the opposite point on the stellar surface from the place where the bubble broke out, compresses the unburnt surface layers there, and initiates a detonation (Plewa et al. 2004; Plewa 2007; Townsley et al. 2007). Figures 1 and 2 illustrate these different stages in the 18b42o6r simulation. The image in Figure 3 is identical to that in Figure 2 (*bottom right*), except that we have rotated the star to show the very hot ($T > 3 \times 10^9$ K) region at the head of the inward jet that has reached densities greater than 2×10^7 g cm $^{-3}$, conditions that exceed conservative criteria for initiation of a detonation (Niemeyer & Woosley 1997; Röpke et al. 2007).

We compare the nuclear energy, E_{nuc} , released during the deflagration phase as a function of time for the 18b42o6r and 16b40o8r simulations, and the 25b100o6r and 25b100o8r simulations, in the left panel of Figure 4. In both cases, the curves for the two different resolutions are in close agreement. This result is expected if buoyancy-driven nuclear burning depends mostly on the fluid dynamical behavior at larger scales. As remarked earlier, such a picture is suggested by the results of Zhang et al. (2007), who find that the time-averaged rate of buoyancy-driven nuclear burning did not vary when the resolution was varied by a factor of 4. However, this is an open question, as discussed in § 2, and further studies are needed in order to answer it.

We compare the nuclear energy released, E_{nuc} , as a function of time for the 16b20o8r, 16b40o8r, 16b100o8r, 25b100o8r, and 50b100o8r simulations in the right panel of Figure 4. The first three form a sequence in which both the time at which the curves flatten and the amount of nuclear energy E_{nuc} that is released decreases as the offset distance r_{offset} of the ignition region increases. This behavior is similar to that found by Townsley et al. (2007) in their 2D simulations of the GCD model.

The unburnt surface material in the initial collision region reaches $T > 3 \times 10^9$ K, but densities of only $\rho \sim 10^5$ – 10^6 g cm $^{-3}$, which are insufficient to produce a detonation (Niemeyer & Woosley 1997). The collision, however, produces inward- and outward-directed jets. The outward jet ejects material at velocities $v_{\text{jet}} \sim 40,000$ km s $^{-1}$. The inward jet impacts the stellar surface, stalls, and spreads a little. This sequence of events compresses the hot ($T > 3 \times 10^9$ K) material ahead of the jet to densities $\rho > 1 \times 10^7$ g cm $^{-3}$, and in some cases even $\rho > 2 \times 10^7$ g cm $^{-3}$. These conditions exceed conservative conditions for initiation of a detonation (Niemeyer & Woosley 1997; Röpke et al. 2007). As

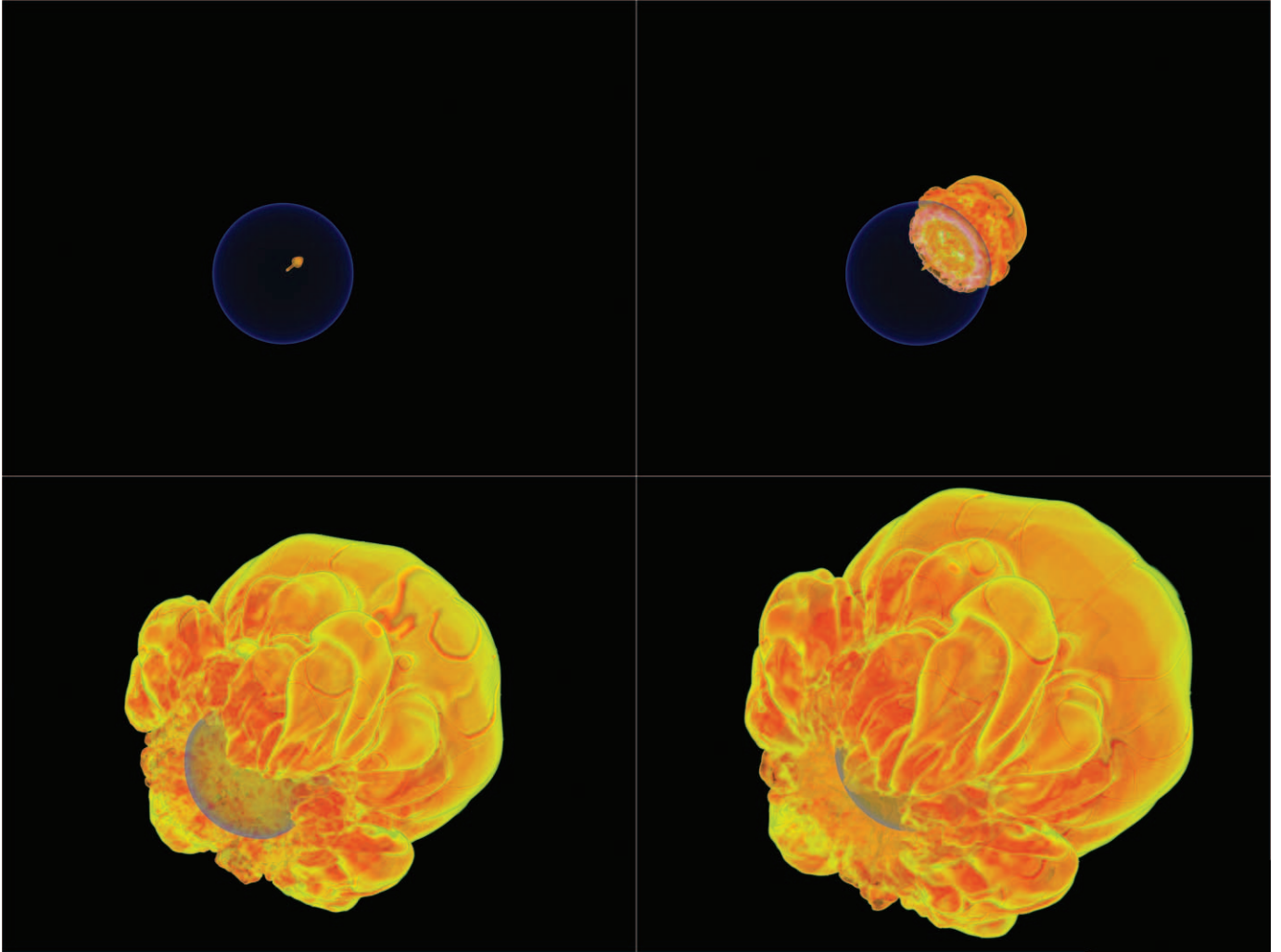


FIG. 1.—Images showing the hot ash and the star at different times for the 6 km resolution simulation of the GCD model starting from initial conditions in which a 25 km radius initial bubble offset 100 km from the center of the star. The images show volume renderings of the surface of the star [defined as the region in which $\rho = (1.5\text{--}2.0) \times 10^7 \text{ g cm}^{-3}$] and the flame surface (defined as the surface where the flame progress variable $\phi_1 = 0.5$) at: 0.5 s, soon after the bubble becomes R-T unstable and develops into a mushroom shape (*top left*); 1.0 s, as the bubble breaks through the surface of the star (*top right*); 1.5 s, when the hot ash is flowing over the surface of the star (*bottom left*); and 1.7 s, shortly before the hot ash from the bubble collides at the opposite point on the surface of the star (*bottom right*).

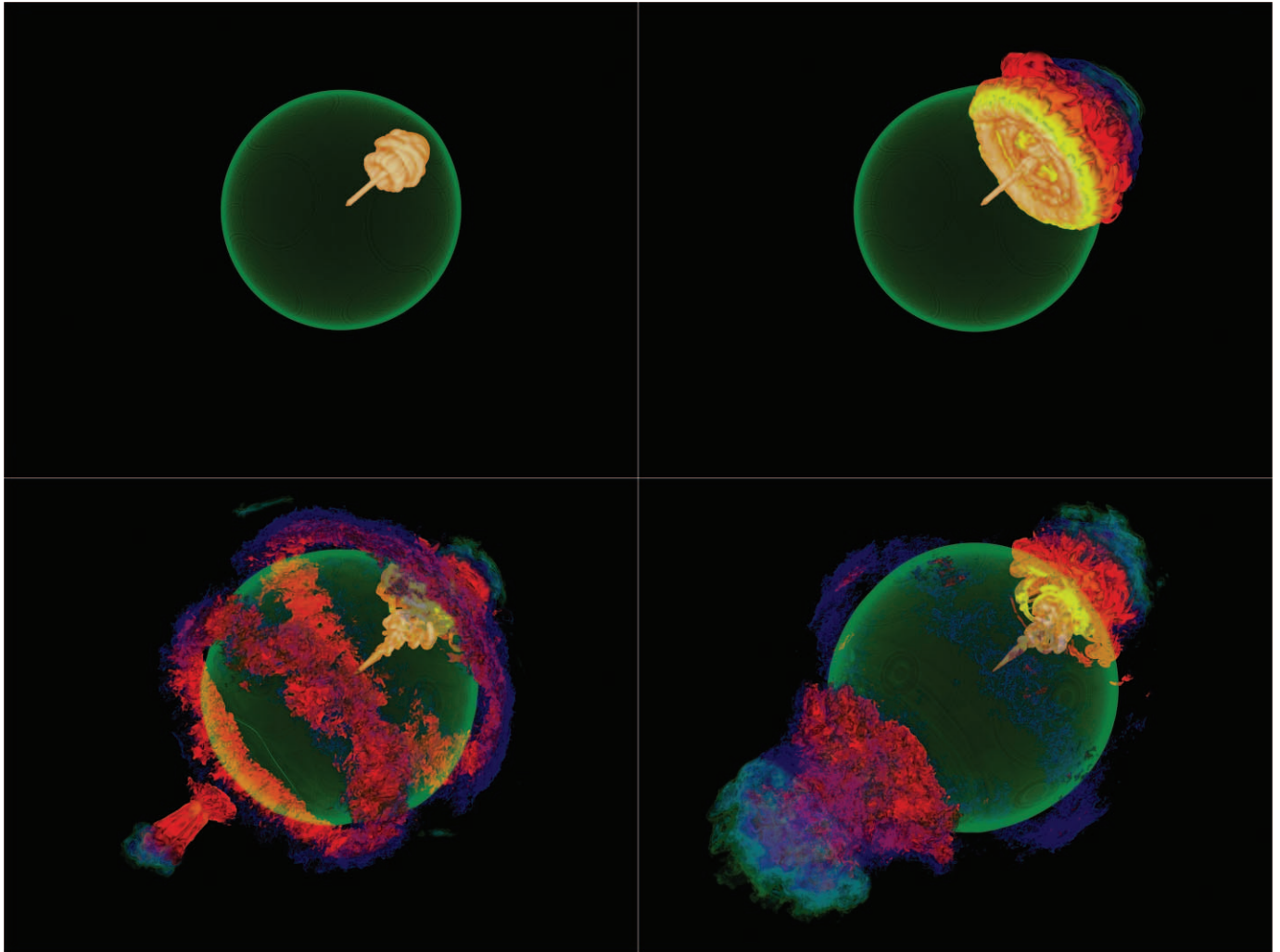


FIG. 2.—Images showing very hot matter and the star at different times for the same simulation as in Fig. 1. The images are volume renderings of the surface of the star [defined as the region in which $\rho = (1.5\text{--}2.0) \times 10^7 \text{ g cm}^{-3}$] and the regions where the temperature is very high [i.e., where $T = (1.5\text{--}4.0) \times 10^9 \text{ K}$, and blue is the coolest and orange-white is the hottest temperature] at: 0.8 s, when the bubble has become R-T unstable and developed into a mushroom shape (*top left*); 1.0 s, as the bubble breaks through the surface of the star (*top right*); 1.7 s, shortly before the hot ash from the bubble collides at the opposite point on the surface of the star (*bottom left*); and 1.84 s, the moment when the inward jet has compressed and heated stellar material ahead of it to detonation conditions (*bottom right*).

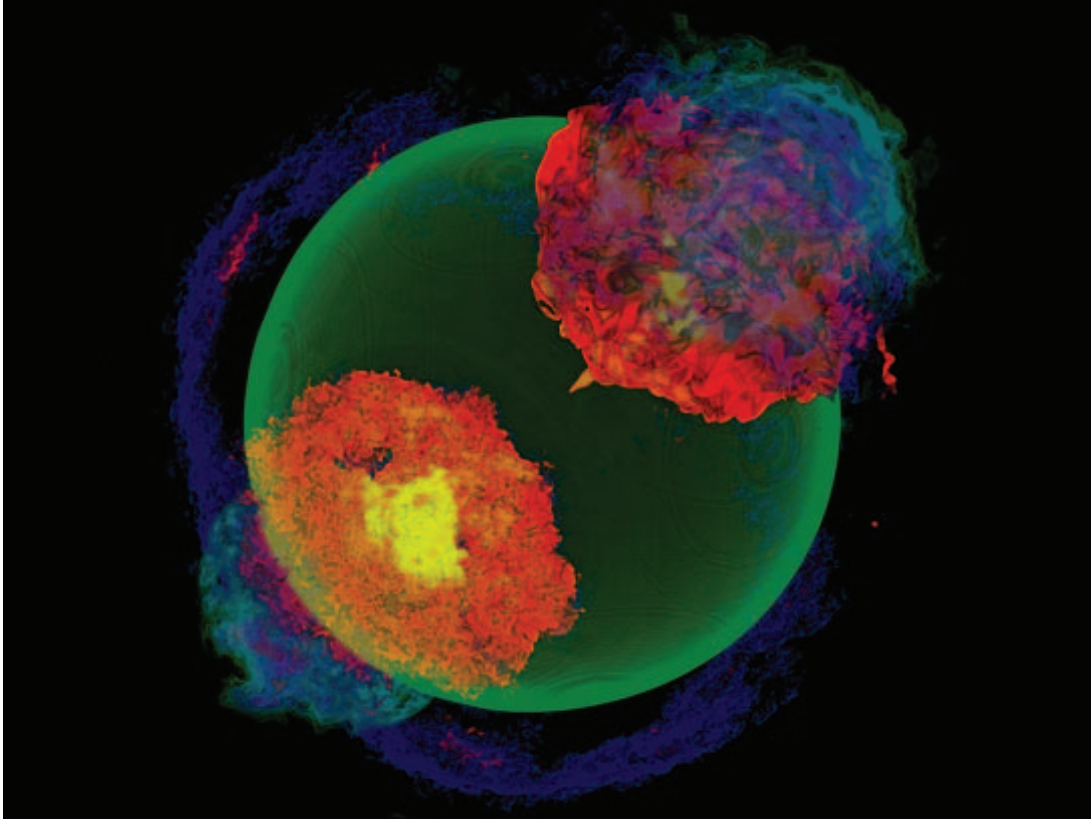


FIG. 3.—Same image as that in Fig. 2 (*bottom right*), except that we have rotated the star to show the face of the inward-directed jet where conditions for detonation are robustly achieved.

we will report in a later paper, subsequent 3D simulations of the GCD model we have carried out that include nuclear burning outside the flame detonate, and inclusion of such burning does not significantly alter the time at which the detonation occurs compared to the first moment at which the simulations reported in the

present paper reach conditions for detonation (G. C. Jordan et al. 2008, in preparation).

The 3D simulations of the GCD model show that, as in our previous 2D simulations (Townsend et al. 2007), it is the kinetic energy originating from the breakout of the bubble of hot ash,

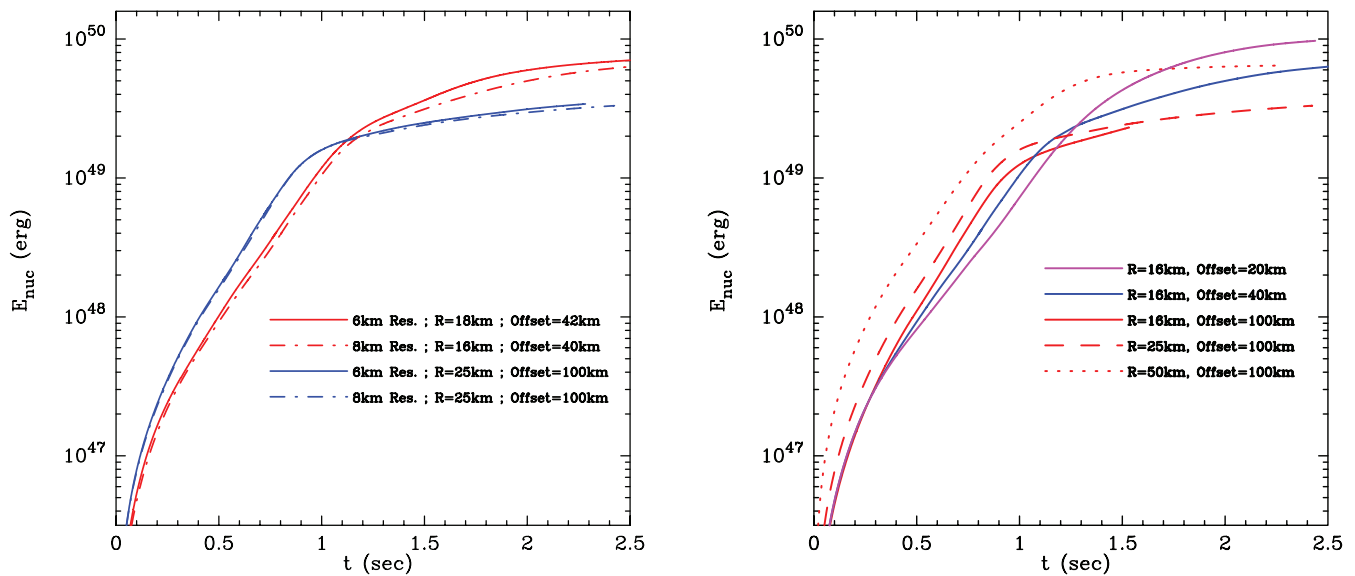


FIG. 4.—Nuclear energy released (E_{nuc}) as a function of time. *Left*: Comparison of 6 and 8 km resolution simulations for two offset distances. Note the close agreement between the two resolutions for both cases. *Right*: Comparison of 8 km resolution simulations for an initial bubble radius of 16 km and three different initial offset distances (20, 40, and 100 km), and for two other initial bubble radii (25 and 100 km) and an initial offset distance of 100 km. Note that the curves for initial bubble radii of 25 km, and especially 50 km—initial conditions that violate the requirement for self-similarity (see text)—are displaced from the other curves, even at early times.

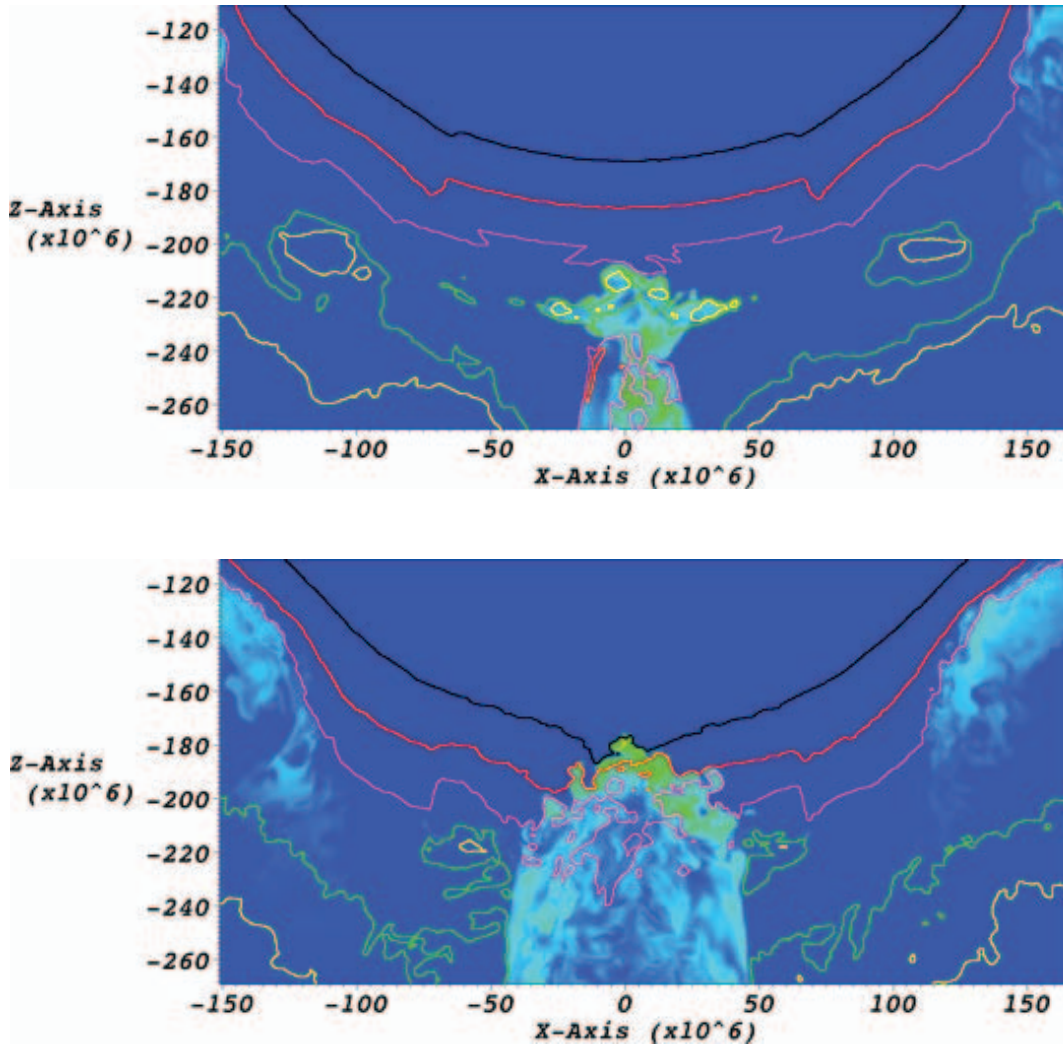


FIG. 5.—Close-up view of 2D slices of the region near the “south pole” of the star. The slices show the inward-directed jet produced by the collision of unburnt material ahead of the hot ash from the bubble in the 25b100o6r simulation just prior to when the density of the material in the hot, inward-directed jet produced by the collision has reached its maximum value. The color shows the temperature, ranging from 1×10^9 to 5×10^9 K from blue through red. The density is indicated by contours. Yellow represents a density of 5×10^5 , green represents 1×10^6 , purple represents 5×10^6 , red represents 1×10^7 g cm^{-3} , and black represents 2×10^7 g cm^{-3} . The color map represents temperature; blue is $T \leq 1.0 \times 10^9$ K, cyan is $T = 2.0 \times 10^9$ K, and green is $T = 3.0 \times 10^9$ K. The units of the axes are centimeters.

imparted to the unburnt surface layers of the star by the inwardly moving jet generated by collision of the surface flows, that causes the unburnt material to achieve the conditions for detonation. This is illustrated in Figure 5, which shows the temperature and density in the collision region in the 18b42o6r simulation just before and just after detonation conditions are reached, and in Figure 3, which is identical to the image in Figure 2 (*bottom right*), except that the star is rotated to show the very hot ($T > 3 \times 10^9$ K) region at the head of the inward jet that has reached densities greater than 2×10^7 g cm^{-3} .

We find that the unburnt material in the surface layers of the star reaches temperatures $T > 2 \times 10^9$ K and densities $\rho > 1 \times 10^7$ g cm^{-3} in all seven 3D simulations we performed, as illustrated in Figure 6. The values of T_{max} and ρ_{max} closely match those in our 2D cylindrical simulations for the same resolution and initial conditions (Townsend et al. 2007). The small difference between the values of T_{max} and ρ_{max} in the 2D and 3D simulations for $r_{\text{offset}} = 20$ km are within the uncertainties we expect in the calculations. Thus, the results of our 2D cylindrical simulations are a good guide to the results of our 3D simulations for the range of initial bubble radii and offset distances, and the resolutions, that we have explored so far.

In order to test the robustness of the GCD mechanism, we ran additional simulations in which we coarsened the resolution in the truncated cone encompassing the collision region from 8 to 16, 32, and 64 km for offset distances of 40 and 100 km. In all cases, the simulations reached the above conservative conditions for detonation. We conclude that, for the initial conditions investigated in this paper, the GCD model robustly achieves temperatures and densities necessary for detonation.

4. DISCUSSION

4.1. Observational Properties of the 3D GCD Model

We have carried out 3D simulations of the GCD model at a finest resolution of 6 km for initial offset distances of 42 and 100 km, and a finest resolution of 8 km for initial offset distances of 20, 42, and 100 km. We find that these simulations robustly reach the conditions necessary for detonation. Vladimirova (2007) and R. Fisher et al. (2008, in preparation) have shown that the evolution of the bubble is self-similar—i.e., its evolution is independent of its initial radius r_{bubble} —provided that $r_{\text{bubble}} < \lambda_c$, where r_{bubble} is the initial bubble radius and λ_c is the minimum wavelength for the unstable R-T growth of flame surface

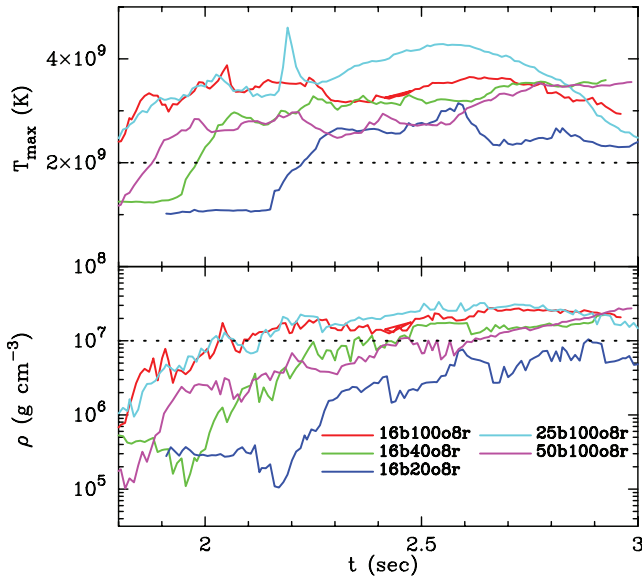


FIG. 6.—Maximum temperature T_{\max} and associated density in the fully refined truncated cone around the “south pole” of the star as a function of time for the five 8 km resolution 3D simulations we performed. The material flowing over the surface of the star enters the lower hemisphere at ~ 1.5 s and collides at ~ 2 s, at which point an inward-directed jet forms. Subsequently, the hot ($T > 3 \times 10^9$ K) material in the jet impacts the surface of the star and becomes compressed, reaching densities $\rho > 1 \times 10^7$ g cm $^{-3}$ in all five of the simulations.

perturbations (see § 2). We find that the bubbles in the simulations in which $r_{\text{bubble}} = 25$ and 50 km at an offset distance $r_{\text{offset}} = 100$ km do not exhibit self-similar behavior, even at early times; i.e., their size and shape at later times differ from each other and from those in the simulation for which $r_{\text{bubble}} = 16$ km (see Fig. 4). This is expected, since in these two simulations the radius of the initial bubble does not satisfy the condition $r_{\text{bubble}} < \lambda_c$ required for self-similar behavior. These two simulations produced larger values of E_{nuc} , but still reached conservative conditions for detonation. Finally, we find that our 3D simulations exhibit a correlation between E_{nuc} and initial offset distance (see Fig. 4), confirming the correlation seen in our 2D cylindrical simulations (Townsend et al. 2007).

Table 1 lists the amount of nuclear energy E_{nuc} released up to a fiducial time of 2 s (which is approximately the time at which a detonation would occur) for the seven simulations reported in this paper. Also listed in Table 1 are estimates of the masses of heavy elements (i.e., iron peak elements) and intermediate-mass elements that are expected to be produced by a subsequent detonation, assuming that the mass of iron peak elements, M_{heavy} , is that at densities above 1.5×10^7 g cm $^{-3}$ and the mass of intermediate-mass elements, M_{inter} , is the mass at densities below this. Finally, Table 1 lists estimates of the expected total energy of the explosion, $E_{\text{total}} = E_{\text{nuc}} + E_{\text{bind}}$, where we estimate E_{nuc} from the masses of heavy and intermediate-mass elements that are produced in each simulation, and E_{bind} is the binding energy of the initial WD model. These results suggest that all of the simulations can be expected to produce large amounts of ^{56}Ni , and therefore very bright and energetic Type Ia supernova explosions, and small amounts of intermediate-mass elements. Thus, these simulations can explain only the brightest and most energetic of the Type Ia supernovae that are observed.

Simulation 50b100o8r, in which the initial bubble has a radius $r_{\text{bubble}} = 50$ km and therefore becomes immediately subject to a strong R-T instability, may crudely mock up what happens if

ignition occurs simultaneously at a cluster of points located off-center in the core of the star. The simulation released more E_{nuc} than did the other two simulations with the same offset distance but with smaller initial bubble radii, and thus suggests a plausible way in which the GCD mechanism could produce more pre-expansion, and therefore much less nickel, yet detonate—i.e., one way in which the GCD mechanism might account for less luminous Type Ia supernovae. However, this is an open question, which we plan to explore in a future paper.

An essential aspect of the GCD model is that, while the nuclear energy released during the deflagration phase causes the star to expand prior to the detonation, it leaves the majority of the star unburnt and undisturbed, as we have shown in earlier work (Plewa et al. 2004; Plewa 2007; Townsley et al. 2007) and in this work. The subsequent detonation phase can therefore be expected to produce a smooth, stratified compositional structure in the interior of the star similar to that inferred from spectroscopic observations of Type Ia supernovae, and something that 2D cylindrical and 3D simulations of both the pure deflagration model (Höfllich et al. 2002; Leonard et al. 2005; Badenes et al. 2006; Wang et al. 2006, 2007), and the DDT model (see, e.g., Gerardy et al. 2007) have difficulty in doing. As is evident in Figures 1 and 2, the GCD model also produces turbulence and compositional inhomogeneities in the outermost layers of the star, which appear capable of matching properties inferred from observations of line polarization in the optical (Wang et al. 2006, 2007) and line profiles in the near-infrared (NIR) and mid-infrared (MIR) (Gerardy et al. 2007).⁸ Thus, the pure deflagration and DDT models predict an inhomogeneous, mixed composition in the core and a uniform composition in the outermost layers of the star—a compositional structure that is opposite to that inferred from observations, while the GCD mechanism predicts a smoothly stratified composition in the core and an inhomogeneous, mixed composition in the outermost layers of the star, which agrees qualitatively with the compositional structure inferred from observations.

4.2. Comparison with Other Work

Röpke et al. (2007) have recently conducted an extensive set of 2D cylindrical simulations and a few 3D simulations of the deflagration phase of the GCD model. They find that the conditions for detonation are reached for a number of their 2D cylindrical simulations for a variety of initial conditions. However, the 3D simulations they performed did not reach conditions for detonation, whereas our 3D simulations do.

In an effort to understand the origin of this difference, we carried out 6 and 8 km resolution simulations for exactly the same initial conditions as were used for one of the two Röpke et al. (2007) 3D simulations in which ignition was posited to occur at a single point: an initial spherical bubble of radius 25 km offset a distance of 100 km from the center of the star (see above).⁹ We also carried out an 8 km resolution simulation with an initial bubble radius $r_{\text{bubble}} = 50$ km and an offset distance $r_{\text{offset}} = 100$ km. In all cases, the simulations reached conservative conditions for detonation, as we have described above. The results

⁸ It should be noted that one of the two events discussed in Gerardy et al. (2007) is a subluminous Type Ia supernova, whereas the GCD simulations reported in this paper produce very bright Type Ia supernovae.

⁹ We did not simulate the other initial conditions, for which Röpke et al. (2007) did a 3D simulation positing a single ignition point (i.e., an initial bubble radius of 25 km and an offset distance of 200 km) because these initial conditions lie far above the $r_{\text{bubble}} = \lambda_c$ curve, and are therefore not physically self-consistent (R. Fisher et al. 2008, in preparation).

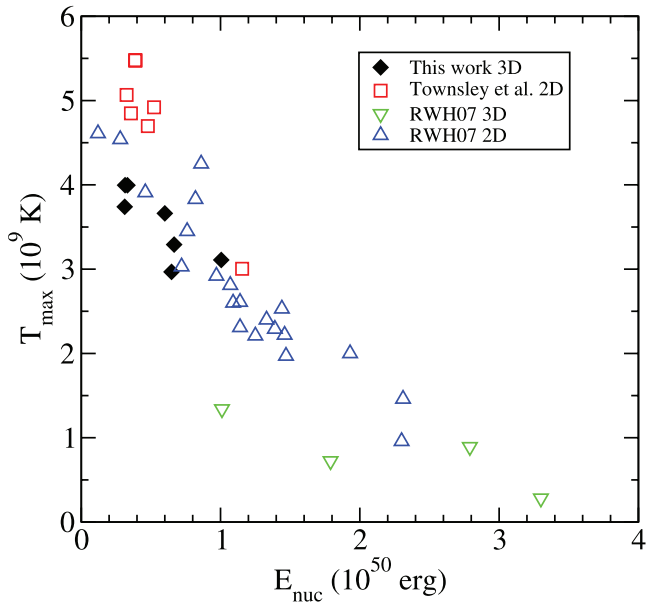


FIG. 7.—Locations in the $(E_{\text{nuc}}, T_{\text{max}})$ -plane of our 2D and 3D simulations of the GCD model and of Röpke et al.’s (2007) 2D and 3D simulations of the same model. The four diamonds are (from left to right) the locations of our 25b100o6r and 25b100o8r simulations (for which the diamonds almost completely overlap) and our 16b40o8r and 18b42o6r simulations. Note the correlation between E_{nuc} and T_{max} reported by Röpke et al. (2007).

provide evidence of the ability of the GCD model to produce the conditions for detonation for a range of initial conditions, but leave unanswered the question of why Röpke et al. (2007) find that the criteria for detonation are reached for a range of initial conditions in their 2D simulations but not in the 3D simulations that they performed, whereas we find that the criteria for detonation are satisfied for a range of initial conditions in our 2D simulations (Townesley et al. 2007) and in our 3D simulations, as reported in this paper.

We show the values of T_{max} and E_{nuc} for both the current 3D models and our previous 2D models (Townesley et al. 2007), and the 2D and 3D models of Röpke et al. (2007) in Figure 7. This figure shows that there is a relation between T_{max} in the collision region and E_{nuc} . Such a relation is expected in the GCD model to the degree that larger values of E_{nuc} produce more preexpansion of the WD, and therefore less kinetic energy in the flow of hot bubble material over the stellar surface, leading to lower values of the temperature in the collision region. The amount of preexpansion of the star can be expected to depend on when the nuclear energy is released, as well as how much is released. The fact that the relation between T_{max} in the collision region and E_{nuc} shown in Figure 7 is relatively narrow suggests that the amount of nuclear energy that is released is the dominant factor in determining T_{max} .

The results of our 2D cylindrical and 3D simulations for initial conditions consisting of a single, small, spherical bubble offset a range of distances from the center of the star agree with each other, as previously noted, and lie on the relation between T_{max} and E_{nuc} . So do the results of Röpke et al.’s (2007) 2D cylindrical simulations for initial conditions consisting of a cluster of bubbles and for two teardrop-shaped ignition regions located on opposite sides of the center of the star, as well as a single spherical bubble, all offset a range of distances from the center of the star. The results of their 3D simulations for initial conditions consisting of a single bubble also follow the relation between

T_{max} and E_{nuc} , but those for initial conditions consisting of a cluster of bubbles and for two teardrop-shaped ignition regions located on opposite sides of the center of the star do not. In particular, their 3D simulations starting with a cluster of bubbles release a low enough E_{nuc} that they should reach detonation conditions if the relation between T_{max} and E_{nuc} were followed. Most importantly, Röpke et al. (2007) make no mention of the outward-directed jet, and especially the inward-directed jet, which we find plays a crucial role in achieving detonation conditions. Consequently, it is difficult to make direct comparisons between our simulations and theirs.

The main conclusion we draw from Figure 7 is that the amount of E_{nuc} released in Röpke et al.’s (2007) 2D simulations is more, and in Röpke et al.’s 3D simulations is much more, than is released in our 2D Townesley et al. (2007) and 3D simulations, which release similar amounts of E_{nuc} for the same initial conditions and resolution. Consequently, the kinetic energy of the surface flow in their 3D simulations—as measured by T_{max} —is much smaller, and the simulations do not achieve detonation conditions.

Without knowledge of the details of their simulations, it is difficult to know why the results of their 3D simulations differ from those of their 2D simulations, which—while releasing more E_{nuc} —lead to a surface flow similar to what we see in our 2D and 3D simulations. A likely reason is the different treatments of buoyancy-driven turbulent nuclear burning in their simulations and in ours. Our treatment assumes that the rate of buoyancy-driven turbulent nuclear burning depends mostly on the behavior of the flow at larger scales. As we have seen, this provides an explanation for why the results of our 2D and 3D simulations agree. It may also provide an explanation for why the results of Röpke et al.’s (2007) 2D simulations agree with our 2D (and therefore also our 3D) simulations: their treatment of buoyancy-driven turbulent nuclear burning uses the properties of the flow at scales above the grid scale of the simulation to determine the turbulent energy at subgrid scales, and therefore the increase in the nuclear burning rate (which is parameterized as an increase in the value of the flame speed) due to this turbulence. The fact that turbulence in 3D leads to a cascade of smaller and smaller eddies, while turbulence in 2D does not, means that their treatment of buoyancy-driven turbulent nuclear burning does not increase the rate of nuclear burning in 2D, whereas in 3D it will. The origin of the similarities between our 2D and 3D results and Röpke et al.’s (2007) 2D results, and the difference between these results and Röpke et al.’s 3D results, are thus most likely due to differences in the treatment of buoyancy-driven turbulent nuclear burning. As we have noted above, the appropriate treatment of such burning is an open question, and is—as the above differences emphasize—an important topic for future study.

5. CONCLUSIONS

We have conducted a series of 3D simulations of the GCD mechanism for several offset distances and resolutions. Conservative conditions necessary for detonation are robustly achieved in all cases. The initial conditions explored in this paper lead to conditions at detonation that can be expected to produce large amounts of ^{56}Ni and small amounts of intermediate-mass elements. These particular simulations are therefore relevant only to high-luminosity Type Ia supernovae. We find a correlation between the central density of the star at detonation, and both the offset distance and the radius of the initial bubble. These correlations offer a possible explanation for the observed variation in nickel mass in Type Ia supernovae. Finally, the uniform,

homogeneous cores and the turbulent, heterogeneous composition of the outer layers of the stars at the time when the conditions for detonation are reached match the properties inferred from recent polarization, NIR, and MIR observations of Type Ia supernovae.

The authors thank Nathan Hearn for discussions of this work and for his software analysis tools, which were invaluable in the preparation of this paper. The authors thank the code group in the Flash Center, especially Anshu Dubey, Lynn Reid, Paul Rich, Dan Sheeler, and Klaus Weide, for development of the code and for help in running our large simulations on uP at LLNL. We also thank Brad Gallagher and the visualization group in the Flash Center for creating the images used in Figures 1, 2, and 3, and the

corresponding movies; and Hank Childs and the VisIt team at LLNL for help in using VisIt. Finally, we thank LLNL Computing for help in running our large simulations on uP at LLNL, and the NERSC support staff at LBNL for help in running them on Bassi and Seaborg. This work is supported in part at the University of Chicago by the US Department of Energy (DOE) under contract B523820 to the ASC Alliances Center for Astrophysical Nuclear Flashes, and in part by the National Science Foundation under grant PHY 02-16783 for the Frontier Center Joint Institute for Nuclear Astrophysics (JINA). This research used computational resources awarded under the INCITE program at LBNL NERSC, which is supported by the Office of Science of the US Department of Energy under contract DE-AC03-76SF00098. A. C. C. acknowledges support from NSF grant ST-0507456. J. W. T. acknowledges support from Argonne National Laboratory, which is operated under DOE contract W-31-109-ENG-38.

REFERENCES

- Badenes, D. C., et al. 2006, *ApJ*, 645, 1373
 Bravo, E., & Garcia-Senz, D. 2006, *ApJ*, 642, L157
 Calder, A. C., et al. 2002, *ApJS*, 143, 201
 ———. 2004, preprint (astro-ph/0405162)
 ———. 2007, *ApJ*, 656, 313
 Fryxell, B., et al. 2000, *ApJS*, 131, 273
 Gamezo, V. N., Khokhlov, A. M., & Oran, E. S. 2004, *Phys. Rev. Lett.*, 92, 211102
 ———. 2005, *ApJ*, 623, 337
 Gamezo, V. N., et al. 2003, *Science*, 299, 77
 Gerardy, C., et al. 2007, *ApJ*, 661, 995
 Höflich, P., et al. 2002, *ApJ*, 568, 791
 Khokhlov, A. M. 1991, *A&A*, 245, 114
 ———. 1995, *ApJ*, 449, 695
 Leonard, D. C., et al. 2005, *ApJ*, 632, 450
 Livne, E., Asida, S. M., & Höflich, P. 2005, *ApJ*, 632, 443
 Niemeyer, J. C. 1999, *ApJ*, 523, L57
 Niemeyer, J. C., & Woosley, S. E. 1997, *ApJ*, 475, 740
 Perlmutter, S., et al. 1998, in *Abstracts of the 19th Texas Symposium on Relativistic Astrophysics and Cosmology*, ed. J. Paul, T. Montmerle, & E. Aubourg (Paris: CEA Saclay), 146
 Plewa, T. 2007, *ApJ*, 657, 942
 Plewa, T., Calder, A. C., & Lamb, D. Q. 2004, *ApJ*, 612, L37
 Reinecke, M., et al. 1999, *A&A*, 347, 724
 ———. 2002a, *A&A*, 386, 936
 ———. 2002b, *A&A*, 391, 1167
 Riess, A., et al. 1998, *AJ*, 116, 1009
 Röpke, F., & Hillebrandt, W. 2005, *A&A*, 431, 635
 Röpke, F., Niemeyer, J. C., & Hillebrandt, W. 2003, *ApJ*, 588, 952
 Röpke, F., Woosley, S. E., & Hillebrandt, W. 2007, *ApJ*, 660, 1344
 Schmidt, W., Niemeyer, J. C., & Hillebrandt, W. 2006a, *A&A*, 450, 265
 ———. 2006b, *A&A*, 450, 283
 Timmes, F. X., & Woosley, S. E. 1992, *ApJ*, 396, 649
 Townsley, D., et al. 2007, *ApJ*, 668, 1118
 Vladimirova, N. 2007, *Combust. Theory Modelling*, 11, 377
 Vladimirova, N., Weirs, G., & Ryzhik, L. 2006, *Combust. Theory Modelling*, 10, 727
 Wang, L., et al. 2006, *ApJ*, 653, 490
 ———. 2007, *Science*, 315, 212
 Woosley, S. E., Wunsch, S., & Kuhlen, M. 2004, *ApJ*, 607, 921
 Wunsch, S., & Woosley, S. E. 2004, *ApJ*, 616, 1102
 Zhang, J., et al. 2007, *ApJ*, 656, 347
 Zingale, M., et al. 2005, *ApJ*, 632, 1021